
Article:
Xiao, S. and Griffo, A. orcid.org/0000-0001-5642-2921 (2020) PWM-based flux linkage and rotor temperature estimations for permanent magnet synchronous machines. IEEE Transactions on Power Electronics, 35 (6). pp. 6061-6069. ISSN 0885-8993

https://doi.org/10.1109/tpel.2019.2948578

PWM-based Flux Linkage and Rotor Temperature Estimations for Permanent Magnet Synchronous Machines

Shuai Xiao, Antonio Griffo, *Member, IEEE*
Department of Electronic and Electrical Engineering, The University of Sheffield, Sheffield, UK

***Abstract*—Monitoring of rotor temperature in permanent magnet synchronous machines (PMSM) is of great significance as high temperatures can cause partial or even irreversible demagnetization of the permanent magnets. Rotor temperature measurement unfortunately is particularly difficult in practice, since it is difficult to access temperature sensors on a rotating shaft. Nevertheless, rotor temperature can be predicted indirectly with the information of rotor magnet flux linkage, as permanent magnet (PM) remanence decreases with rotor temperature. In this paper, a simple and relatively accurate method for online estimation of PM flux linkage is presented, based on the measurement of current response to the standard space-vector pulse width modulation (SV-PWM). This method uses the already-existing PWM voltage as the excitation signal in order to avoid of the need for additional signal injection. Knowledge of machine parameters, such as inductances which may vary due to saturation, is not required. The proposed methodology is experimentally verified and applied to rotor temperature prediction.[1]**

***Keywords*—PM flux linkage, PMSM, Rotor temperature, SV-PWM**

I. Introduction

Permanent magnet synchronous machines (PMSMs) are widely popular in servo and traction applications due to their high torque and power density. Their use in applications where high reliability must be guaranteed requires careful online condition monitoring of the motor [1]. Thermal monitoring of the machine is particularly important, since temperature is typically the main environmental stressor causing state-of-health degradation and ultimate failure. In terms of motor stators, several direct and indirect temperature monitoring techniques are well established. Temperature sensors such as thermistors and thermocouples can be relatively easily embedded into machine stators during the manufacturing process. However, the requirement for additional sensors may increase costs. Rotor temperature monitoring is of equal importance as high temperature increases the risk of partial, or even total irreversible demagnetization of rotor magnets [2]. Rotor temperatures are difficult to measure in practice, as the rotating shaft can only be accessed through slip rings [3], infrared [4], [5] or other wireless sensors [6], [7], making direct measurement unrealistic in most applications. Hence model-based methods, have been investigated in recent years.

One of the most commonly employed approaches is based upon the use of a lumped parameter thermal network (LPTN). It can be the basis for a thermal 'observer' which, combined with loss models, is capable of providing accurate temperature estimation during real-time operation. Two multi-node thermal models for PMSM are presented in [8], [9]. They are able to predict the temperatures in a number of locations within the machine. However, the models require information on the internal topology, materials and interfaces between them which might not be directly available in practical applications. Low-order LPTNs [1], [10] and [11] lump large regions of the machine in few nodes and detailed knowledge of the motor internal topology, materials and dimensions might not be required if measurement-based parameter identification procedures, which determine the values of the thermal parameters based on the minimization of a specified cost function, are used [12].

As an alternative to model-based estimation, it is also possible to determine motor temperatures via temperature dependent electrical parameters. In [13] rotor temperature is estimated by measuring the response to the injection of a pulsating high-frequency current signal to the *d*-axis of the PMSM noting that the resulting high-frequency resistance changes with rotor temperature. Rotor temperature can also be potentially acquired indirectly from the estimation of rotor magnet flux linkage, as NdFeB PM loses approximately 0.1% remanence per one degree Celsius temperature rise [14]. A number of methods regarding PM flux linkage estimation have been presented in publications based on signal injection techniques. Ref. [15] proposes an online method to estimate stator resistance and rotor PM flux linkage under constant load torque with two sets of *dq*-axis voltage equations corresponding to $i_d = 0$ and the injection of a $i_d \neq 0$ test signal. Compared to [16]-[18], it does not require the knowledge of the nominal values of any unknown parameters in the voltage equation, which may differ from their real values, and its accuracy is not

The authors are with the Electrical Machines and Drives Research Group, Department of Electronic and Electrical Engineering, The University of Sheffield, Sheffield, S1 4DE, U.K. (email: sxiao7@sheffield.ac.uk; a.griffo@sheffield.ac.uk).

affected by the variation in motor parameters due to $i_d \neq 0$. Likewise, by utilizing a zero-voltage injection scheme, flux linkage is directly determined with the measurement of the average value of the voltage commands which are the output of current loop PI controllers of the standard field-oriented control at different rotor speed [19]. In both methods, the *dq*-axis inductance terms are cancelled during the derivation of the methods, resulting in a parameter-independent estimation. However, signal injection-related methods are not desirable because the additional signal disturbs the motor performance by producing additional current and thus additional torque ripples and additional losses. The use of rotor flux linkage model-based observer is proposed in [2], [20] and [21], which is able to accurately predict PM temperature. Nevertheless, this method is difficult to apply practically, because of the necessity of a precise modelling for motor and inverter — the model-related errors otherwise will be misinterpreted as temperature changes. Flux linkage can also be identified with motor armature current and voltage measured by a digital power meter, as introduced in [22]. However, such equipment can be expensive. In addition, ref. [23] and [24] present a new estimation scheme involving the use of curve-fitting parameter identification algorithm, such as recursive least squares (RLS), and extended Kalman Filter (EKF). As a result, the values of flux linkage can be updated continuously in real-time.

This paper presents a relatively simple and accurate method for online flux linkage and rotor temperature estimations, which only involve the measurements of motor phase voltages and currents in response to the standard SV-PWM. Similarly to [15], [19], knowledge of inductances is not required for the estimations. Furthermore, this method does not need signal injection as the excitation signal is intrinsic in the PWM voltage. The principle of the proposed method was presented in [25], but only demonstrated through computer and real-time simulation using Hardware-in-the-Loop (HIL) techniques. This paper, expanding on [25], provides extensive experimental validations as well as detailed analyses of the main sources of errors in practical applications.

The main contributions of this paper include:

- A detailed analysis of the robustness of this method against a number of practical implementation issues, including inverter nonlinearity due to dead-time.
- A comprehensive experimental validation of the methodology conducted on a three-phase surface-mounted PMSM (SPMSM). Relatively small errors in the flux linkage and rotor temperature estimations in a variety of motor operating conditions and temperatures are achieved.

II. Fundamental Theory

Flux linkage is assumed to be linearly dependent on rotor temperature as:

$$\psi_m(T) = \psi_m(T_{ref})[1 + \alpha_{\beta r}(T - T_{ref})] \tag{1}$$

where $\psi_m(T)$ and $\psi_m(T_{ref})$ are the flux linkages at the rotor and reference temperatures; $\alpha_{\beta r}$ is a temperature-dependent coefficient, which for the most widely used NdFeB magnet is approximately $-0.12\%/°C$. The rotor temperature can then be calculated as:

$$T = T_{ref} + \frac{1}{\alpha_{\beta r}}\left[\frac{\psi_m(T)}{\psi_m(T_{ref})} - 1\right] \tag{2}$$

It is clear that the accuracy of the flux linkage estimation strongly influences the rotor temperature estimation due to the small temperature coefficient $\alpha_{\beta r}$ at the denominator in (2). Fig. 1 shows the magnet flux linkage as function of temperature for the experimentally tested SPMSM in this paper. It is clear that the temperature coefficient has a small nonlinearity with temperature which will need to be taken into account for accurate temperature prediction.

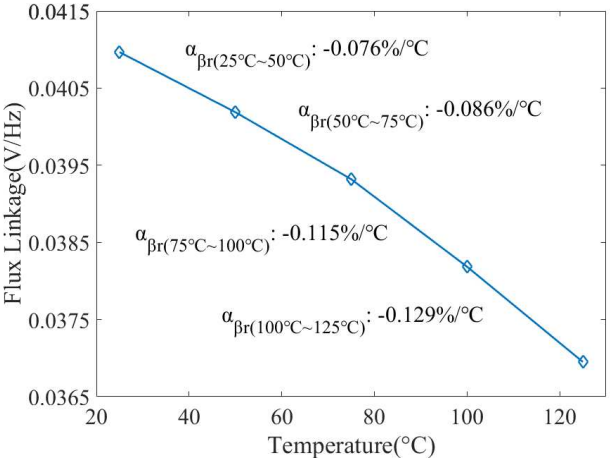

Fig. 1: The values of $\alpha_{\beta r}$ at each temperature region for the tested motor

Assuming a relatively small value of $\alpha_{\beta r} = -0.076\%/°C$, an 1% error in the flux linkage could result in a $13°C$ error in the rotor temperature estimation.

The voltage equations of a PMSM represented in rotating *dq*-reference frame are expressed as:

$$v_d = R_s i_d + L_d \frac{d}{dt} i_d - \omega_r L_q i_q \tag{3}$$

$$v_q = R_s i_q + L_q \frac{d}{dt} i_q + \omega_r (L_d i_d + \psi_m) \tag{4}$$

where v_d, v_q, i_d, i_q are the *dq*-axis voltages and currents, respectively; L_d, L_q, R_s are the *dq*-axis inductances as well as the stator resistance, ω_r is the rotor speed, and ψ_m is the rotor PM flux linkage.

In steady-state conditions and assuming $i_d = 0$, rearranging the *q*-axis equation (4) it is possible to calculate the rotor flux ψ_m as:

$$\psi_m = \frac{v_q - R_s i_q}{\omega_r} \tag{5}$$

this simple method, denoted as 'averaged model' in the following, requires the measurements of voltage, current as well as the knowledge of machine parameter R_s. It is evident that the precision of rotor flux estimation relies on the precise knowledge of R_s and the stator voltage. Stator voltages are not commonly measured in motor drives. Although reference voltage could be used, however, dead-times, voltage drops on

the power switches and other inverter non-ideal effects will significantly affect the accuracy of the prediction. The following analysis compares the accuracy of rotor flux estimation based on (5) with a more accurate estimation based on the phase-voltage measurement.

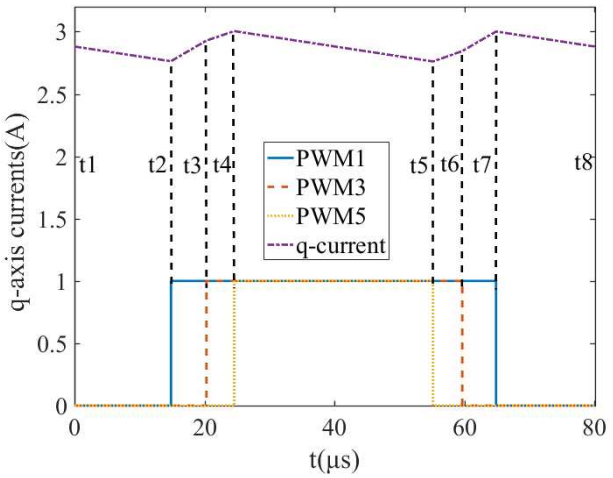

Fig. 2: Gate signals PWM1, PWM3, PWM5, and the corresponding current variation in a single switching period

Fig. 2 shows an example of a single PWM switching period with a duration of $t_{switching} = 1/f_{sw}$, where f_{sw} denotes the switching frequency, PWM1,..,3 being the gate signals controlling the turn-on of the top three devices in a standard two-level voltage-source inverter. $t1 \cdots t8$ are the time instants at which a different voltage vector is applied [26]. The q-axis equation (4) can be discretized with a sampling time $T_s \ll t_{switching}$. The resultant relationships between two adjacent sampling points, assuming the d-axis current to be controlled to zero, are given as:

$$v_{q(t1\sim(t1+T_s))} = R_s i_{q(t1\sim(t1+T_s))} + L_q \frac{d}{dt} i_{q(t1\sim(t1+T_s))} + \omega_r \psi_m \quad (6)$$

$$v_{q((t1+T_s)\sim(t1+2T_s))} = R_s i_{q((t1+T_s)\sim(t1+2T_s))} + L_q \frac{d}{dt} i_{q((t1+T_s)\sim(t1+2T_s))} + \omega_r \psi_m \quad (7)$$

$$\vdots$$

$$v_{q((t1+(n-2)T_s)\sim t8)} = R_s i_{q((t1+(n-2)T_s)\sim t8)} + L_q \frac{d}{dt} i_{q((t1+(n-2)T_s)\sim t8)} + \omega_r \psi_m \quad (8)$$

where T_s is the sampling time, $t1$ is the starting point of the PWM period in Fig. 2, and n is the total number of the sampling points in the period, which must be an integer to guarantee an integer number of equations. The speed ω_r is assumed to be constant during the switching period. The derivative term can be approximated by:

$$di_q/dt \approx \frac{i_{q(t1+(k+1)T_s)} - i_{q(t1+kT_s)}}{T_s} \quad (9)$$

with $k = 0,1 \cdots n-2$. It is noted that the last sampling point in the period is $t8 = t1 + (n-1)T_s$.

When the motor operates at steady-state, the current controller only responds to the currents measured at the beginning of the non-zero active voltage vectors, which are $i_{q(t2)}$ and $i_{q(t5)}$ and ensures that on average they remain constant in steady-state operation. This means $i_{q(t2)} = i_{q(t5)}$, $i_{q(t4)} = i_{q(t7)}$ and also $i_{q(t1)} = i_{q(t8)}$.

Multiplying the $n-1$ equations by dt, which is the sampling time T_s gives:

$$T_s v_{q(t1\sim(t1+T_s))} = T_s R_s i_{q(t1\sim(t1+T_s))} + L_q\left(i_{q(t1+T_s)} - i_{q(t1)}\right) + T_s \omega_r \psi_m \quad (10)$$

$$T_s v_{q((t1+T_s)\sim(t1+2T_s))} = T_s R_s i_{q((t1+T_s)\sim(t1+2T_s))} + L_q\left(i_{q(t1+2T_s)} - i_{q(t1+T_s)}\right) + T_s \omega_r \psi_m \quad (11)$$

$$\vdots$$

$$T_s v_{q((t1+(n-2)T_s)\sim t8)} = T_s R_s i_{q((t1+(n-2)T_s)\sim t8)} + L_q(i_{q(t8)} - i_{q(t1+(n-2)T_s)}) + T_s \omega_r \psi_m \quad (12)$$

Now adding each equation to the next, it yields:

$$T_s \sum_1^{n-1} v_{q(j)} = T_s R_s \sum_1^{n-1} i_{q(j)} + t_{switching} \omega_r \psi_m \quad (13)$$

where j is the j^{th} equation. It can be noticed that the inductance-related terms are eliminated.

With regard to the voltage terms, it is evident that the sum $T_s \sum_1^{n-1} v_{q(j)}$ measured between two adjacent sampling points is always equivalent to the average PWM output voltage:

$$T_s \sum v_q(j) = (t3-t2)v_{q(t3-t2)} + (t4-t3)v_{q(t4-t3)} + (t6-t5)v_{q(t6-t5)} + (t7-t6)v_{q(t7-t6)} \quad (14)$$

It can be easily verified that:

$$(t3-t2)v_{q(t3-t2)} = (t7-t6)v_{q(t7-t6)} \quad (15)$$

$$(t4-t3)v_{q(t4-t3)} = (t6-t5)v_{q(t6-t5)} \quad (16)$$

as the switching period consists of two symmetrical switching combinations. Therefore, (13) now becomes:

$$2\left[(t3-t2)v_{q(t3-t2)} + (t4-t3)v_{q(t4-t3)}\right] = T_s R_s \sum_1^{n-1} i_{q(j)} + t_{switching} \omega_r \psi_m \quad (17)$$

Also, the time differences $(t3-t2)$ and $(t4-t3)$ can be pre-calculated at the beginning of the SV-PWM based on the location of the rotating voltage reference vector on the space vector diagram, and $v_{q(t3-t2)}$ and $v_{q(t4-t3)}$ are the results of the switching vectors being transformed from $\alpha\beta$-reference frame to dq-reference frame. In conclusion, the rotor flux can be calculated as:

$$\psi_m = \frac{f_{sw}}{\omega_r} 2\big[(t3-t2)v_{q(t3-t2)} + (t4-t3)v_{q(t4-t3)}\big] - \frac{f_{sw}}{\omega_r} T_s R_s \sum_{1}^{n-1} i_{q(j)} \quad (18)$$

The voltage reference can be the command voltages generated by the controller in the standard field-oriented control (FOC). However, due to the command voltages being affected by some motor control issues, such as inverter nonlinearity, phase voltages are directly measured and the actual reference calculated from v_{abc} after suitable low-pass filtering.

In addition, the noise level of the flux linkage calculation may be amplified as a result of the estimation of (9). Therefore a low-pass filter with $1Hz$ passband edge frequency is applied to (18), in order to calculate the average flux linkage. Nevertheless the tracking of changes in flux linkage due to temperature will not be affected, as the temperature variation is comparatively slower with typical time constants of many seconds/minutes depending on the size and cooling systems of the motor.

III. Practical Implementation Error Analysis

In practice, flux linkage estimation could be erroneous due to a number of sources of error. The effect of these errors on the proposed methodology can be potentially significant and therefore is evaluated in this section using a simulation model of the experimentally tested SPMSM (parameters specified in Table I) controlled using a standard field-oriented motor control with SV-PWM.

TABLE I
PARAMETERS OF THE SPMSM

Quantity	Unit	Value
Continuous Torque	Nm	0.2754
Max Speed	r/min	6000
DC Link Voltage	V	24
Peak Current	A	7.1
No. of Pole-pairs	--	4
No. of Slots	--	18
Stator Resistance	Ω	0.36
d-axis Inductance	mH	0.1569
q-axis Inductance	mH	0.1569
PM Flux Linkage	V/Hz	0.0409

A. Inverter Dead-time Effect

Inverter dead-time effect is the direct result of a delay time between the opening of the upper switch and the closing of the lower switch, altering the effective output voltage of the motor which is no longer determined only by the reference voltage. Several dead-times ranging from $0.5\mu s$ to $10\mu s$, are applied manually between the three phase PWM and their corresponding complementary signals for the purpose of simulating this particular phenomenon. Fig. 3 plots the flux linkage estimations along with the errors in comparison to the reference.

As can be seen in the figure below, the accuracy of the estimation adopting the simplified method (5) is worsened as dead-time increases, which is the reflection of the increasing difference between the reference and resulting PWM voltages. On the contrary, no more than $\pm 0.01\%$ errors are conceded with PWM-based method, for the reason that the voltage and current are measured and the ones used for motor operations.

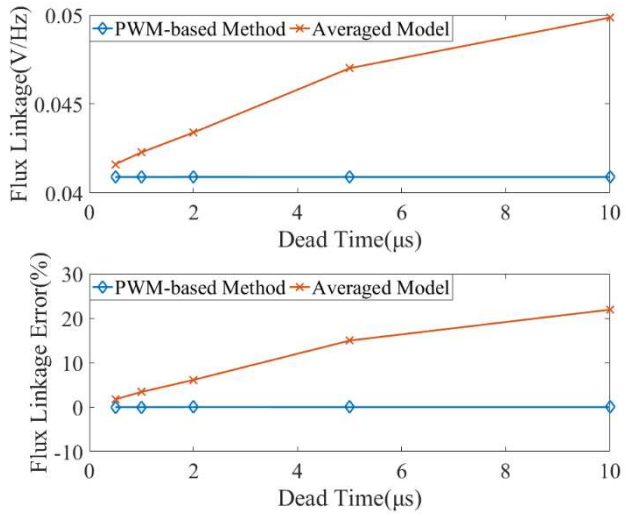

Fig. 3: Flux linkage estimations (top) and the corresponding errors (bottom) with $0.5\mu s$, $1\mu s$, $2\mu s$, $5\mu s$, and $10\mu s$ dead-times applied

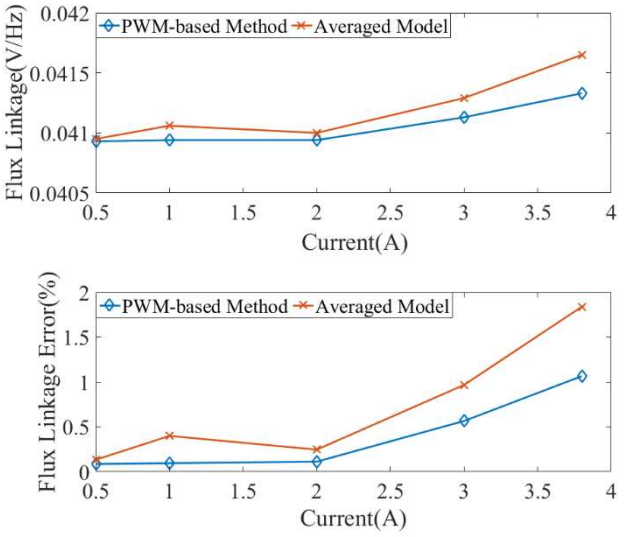

Fig. 4: Flux linkage estimations (top) and the corresponding errors (bottom) at $i_{q\_command} = 0.5A$, $1A$, $2A$, $3A$, and $3.8A$

B. Inductance Saturation

Practically, the main inductances L_d and L_q of PMSMs could be subject to saturation at high current level. The existence of saturation means that the estimation is less precise as the q-axis inductance terms in the voltage equations can no longer be eliminated. The constant inductances in the machine model are replaced with two look-up tables (LUT), which are obtained from the calculations using Finite Element software.

Fig. 4 illustrates the estimation results at $i_{q\_command} = 0.5A, 1A, 2A, 3A, 3.8A$, respectively, showing slightly over 1% error with the PWM-based method and nearly 2% with the simplified method. The inductances of the tested motor in applications in which the current is smaller than $10A$ do not change dramatically. However the data in the LUTs is modified such that the inductance at high current ($5A$) is less than 20% that at low current ($0.5A$) for the purpose of demonstration.

Equations (19) and (20) compensate the voltage errors in (18) and (5), and are used for re-estimating the flux linkage:

$$\psi_m = \frac{f_{sw}}{\omega_r} 2\big[(t3-t2)v_{q(t3-t2)} + (t4-t3)v_{q(t4-t3)}\big] - \frac{f_{sw}}{\omega_r} T_s R_s \sum_{1}^{n-1} i_{q(j)} - \frac{f_{sw}}{\omega_r} \sum_{1}^{n-1} L_{q(j)}\left(i_{q(k+1)} - i_{q(k)}\right) \quad (19)$$

$$\psi_m = \frac{v_q - R_s i_q - \sum L_q \frac{i_{q(m)} - i_{q(m-1)}}{T_s}}{\omega_r} \quad (20)$$

in which: k is the k^{th} sampling point in one PWM switching period and $j = k = 1, 2, \cdots, n-1$, whereas m is the 'current' sampling point in real-time and $m = 2, 3, \cdots \infty$. $L_{q(j)}$ can be acquired from the LUT. The results are shown in Fig. 5, where the improvement on the estimation for both methods is evident. The small deviation in the level of error between the two methods exists, because the small voltage drops across the power switches and shunt resistors are taken into consideration in the inverter model, resulting in a slight mismatch between the reference and PWM voltages.

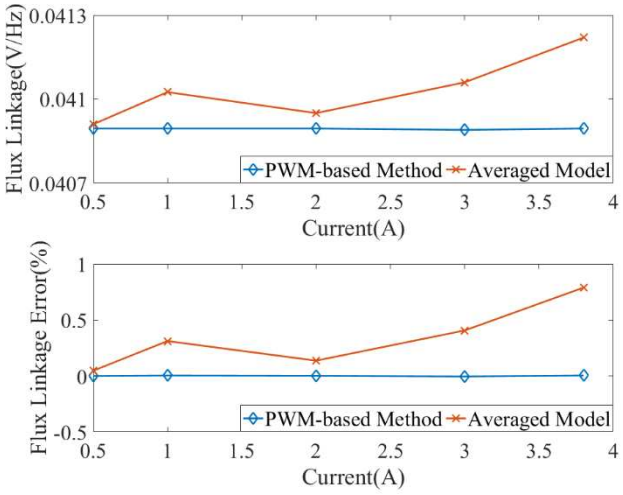

Fig. 5: Flux linkage estimations (top) and the corresponding errors (bottom) after using (19) and (20)

C. Non-zero d-axis current

At $i_d \neq 0$, the precision of the estimation is also affected due to the cancellation of the voltage term $\omega_r L_d i_d$ in (4). The simulation results depicted in Fig. 6 after $i_{d\_command} = -0.5A$, $-1A$, $-1.5A$, $-2A$ and $-3A$ are imposed respectively, show more than -7% error in flux linkage being introduced, using either method. It is assumed that L_d and L_q are their nominal values and remain constant. The estimation error can be compensated by adding the voltage term $\omega_r L_d i_d$ into (18) and (5):

$$\psi_m = \frac{f_{sw}}{\omega_r} 2\big[(t3-t2)v_{q(t3-t2)} + (t4-t3)v_{q(t4-t3)}\big] - \frac{f_{sw}}{\omega_r} T_s R_s \sum_{1}^{n-1} i_{q(j)} - f_{sw} T_s L_d \sum_{1}^{n-1} i_{d(j)} \quad (21)$$

$$\psi_m = \frac{v_q - R_s i_q}{\omega_r} - L_d i_d \quad (22)$$

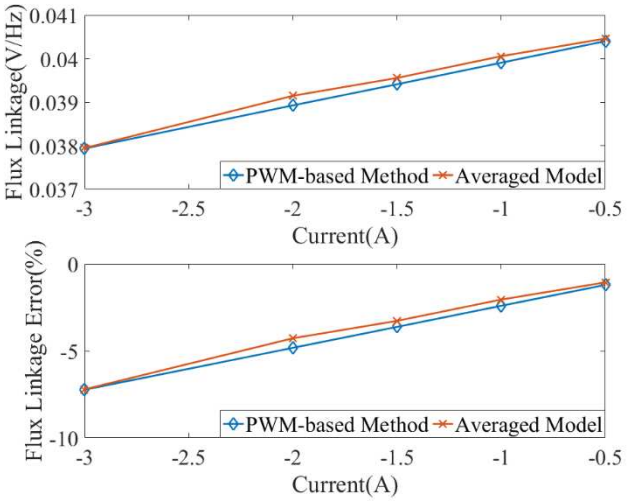

Fig. 6: Flux linkage estimations (top) and the corresponding errors (bottom) at $i_d = -0.5A$, $-1A$, $-1.5A$, $-2A$, and $-3A$

Fig. 7 shows the estimated flux linkage post-compensation, with less than $\pm 0.01\%$ and 0.6% errors demonstrated adopting (21) and (22), respectively.

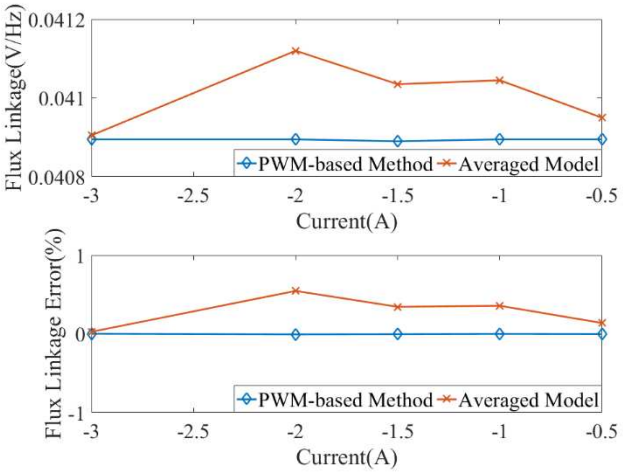

Fig. 7: Flux linkage estimations (top) and the corresponding errors (bottom) post-compensation

IV. Experimental Validation

A. Experimental Setup

Extensive experimental validations have been performed on a two motor dynamometer test rig built with a pair of three-phase PM servo-motors (Teknic M-2310P), with one connected to a three-phase MOSFET inverter and the second serving as a load and working as generator connected with a three-phase resistive load. A quadrature encoder with 4000 counts/rev resolution is used for position measurement. The motor is controlled using a Texas Instruments (TI) C2000 series FOC-enabled microcontroller LAUNCHXL-F28069M LaunchPad. The presented flux linkage estimation algorithm is performed on the FPGA-based data acquisition and control platform OPAL-RT 5600. The code is programmed through RT-LAB, which is a real-time simulation software fully integrated with MATLAB/Simulink.

B. Validation at Room Temperature

As with offline simulation, Fig. 8 exhibits the measured q-axis current variation and the three-phase PWM signals from SV-PWM. It can be noticed that at steady-state conditions, the currents at the beginning of the non-zero voltage periods remain identical because the PI controller regulates the average q-axis current.

The steps shown in the q-axis current in Fig. 8 are the result of the fact that only ten current sampling points are acquired in one PWM switching period. Voltages and currents are acquired at $100\ kS/s$. A switching frequency of $10\ kHz$ for PWM is employed to ensure that the total number of the sampling points, and thus the total number of the equations, in a switching period is integer. However this leads to current ripples as the tested motor has rather small inductances.

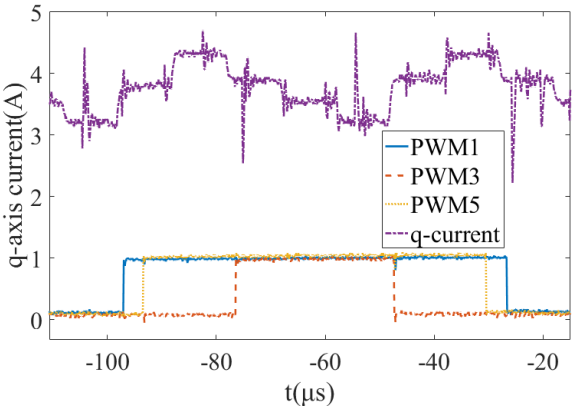

Fig. 8: Three-phase PWM signals and the corresponding q-axis current variation in one switching period in experimental testing

A set of dead-times $0.5\mu s$, $1\mu s$, $2\mu s$, $5\mu s$, and $10\mu s$, are implemented in the inverter to verify the dead-time effect on the presented estimation method. As is seen in Fig. 9, dead-time does not affect the decency of the estimation using the PWM-based method. The controller graphic user interface (GUI) roughly calculates the voltage and current references, with which the flux linkage can also be estimated using (5). The results are in agreement with Fig. 3, as the estimation deteriorates with larger dead-time.

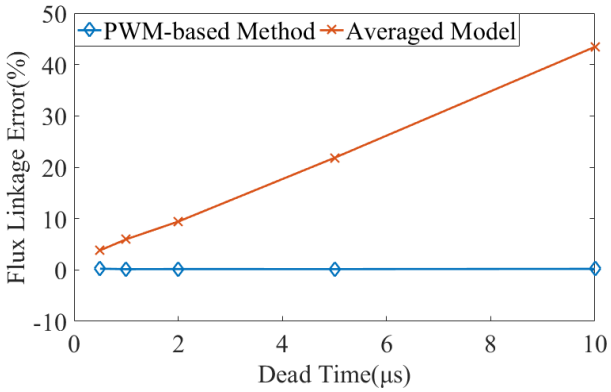

Fig. 9: Flux linkage errors with $0.5\mu s$, $1\mu s$, $2\mu s$, $5\mu s$, and $10\mu s$ dead-times implemented experimentally

C. Validation at Isolated Constant Temperatures

In order to perform tests at various temperatures, the motor is placed in a metal enclosure and wrapped around with two $150\ mm \times 50\ mm$ silicone resistive heater mats powered by $30V$ DC voltage. The mats are connected with a power supply via a temperature controller in which the desired temperatures are set for approximately 30 minutes until the internal thermal equilibrium of the motor is reached. A K-type thermocouple with the sensing tip located at the motor winding is fitted into the controller input module to provide temperature measurement feedback. A simple hysteresis temperature controlled is implemented to reach and maintain the desired winding temperature set-point. This is achieved by using an electromechanical relay which is mounted within the controller and connected to the output pins. The motor is then covered with a calcium-magnesium silicate thermal insulation sheet in order to keep the motor at elevated temperatures and emulate adiabatic thermal conditions. In this way, once thermal equilibrium is reached, it can be assumed that rotor temperature, which is not directly accessible, is very close to the winding temperature which can be directly measured. The setup is shown in Fig. 10.

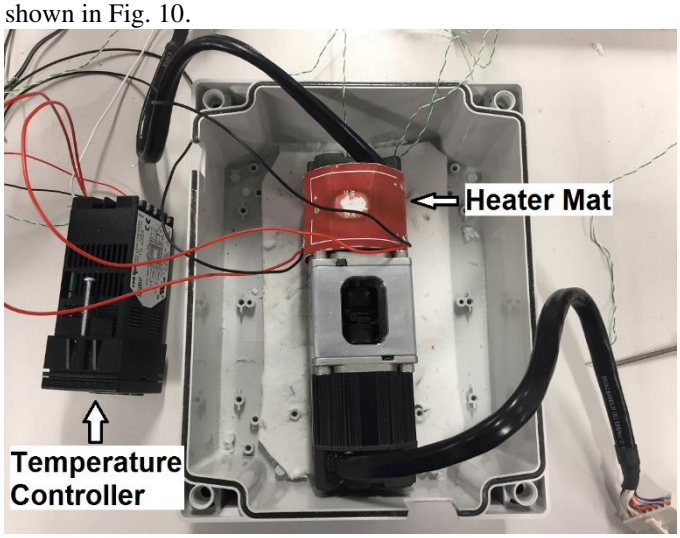

(a)

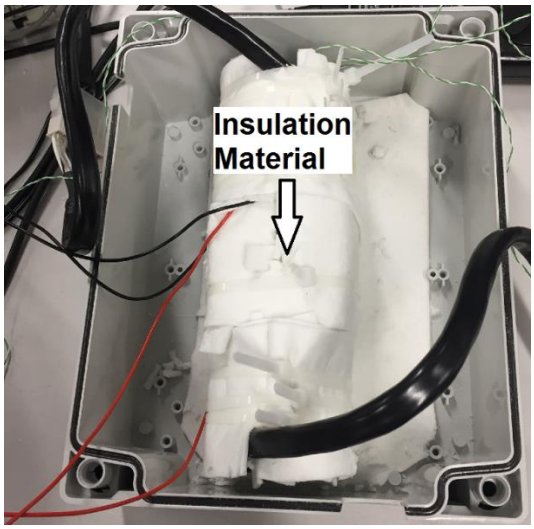

(b)

Fig. 10: (a) Motor wrapped with heater mat and (b) kit wrapped with insulation material

It is important that temperature dependence of stator winding resistance is taken into account in the proposed method. Up to 3% error in flux linkage is detected otherwise at high motor temperatures. It is assumed that the temperature effect on the winding resistance can be described as the following linear function:

$$R_s = R_{s0}[1 + \alpha_T(T_w - T_0)] \tag{23}$$

in which R_{s0} is the phase resistances at a reference temperature T_0, and α_T is a temperature coefficient for copper with the value of $0.393\%/°C$. T_w is the winding temperature which can be measured by thermocouples.

Temperature also affects the B-H curve and permeability of stator core [27], [28], potentially affecting the accuracy of this method. However, as demonstrated in [27] and [28], the temperature effect on the magnetic properties of Silicon-Iron (SiFe) material, used for the tested motor, is small in the typical operating temperatures range for electrical machines (i.e. 20℃ to 120℃) and therefore neglected in the work presented here.

The flux linkage reference is obtained from the phase voltages at no-load condition as:

$$\psi_m = V_{phase}/\omega_r \tag{24}$$

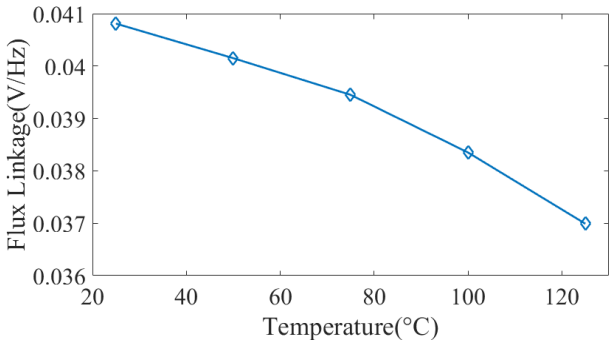

Fig. 11: Flux linkage estimations at 4000rpm and rising temperatures

The estimation results at $4000rpm$ and constant-step elevated motor temperatures starting from $25°C$ are plotted in Fig. 11, where the flux linkage variations are consistent with the inverse relationship between flux linkage and rotor temperature. As shown in Fig. 12, the accuracy of the estimation shows some dependence on motor operating condition (speed) and motor temperature, with the maximum error of -1.3% detected at $1000rpm$ and 125℃. It is also worth mentioning that, as any other 'sensorless' methods for back-EMF/flux linkage estimation, the proposed method shows increasingly poorer performance as the motor speed decreases. This may be related to the presence of speed ω_r at the denominator of (10).

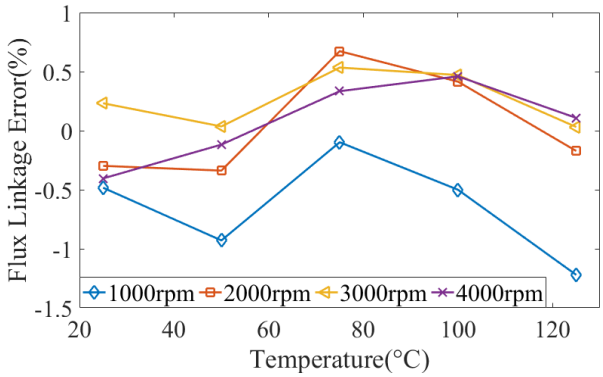

Fig. 12: Flux linkage errors at 1000rpm, 2000rpm, 3000rpm, 4000rpm, and rising temperatures

D. Rotor Temperature Estimation

A calibration procedure has been adopted to evaluate the coefficient $\alpha_{\beta r}$ by measuring the open-circuit back-EMF at different rotor temperatures T_1 and T_2 as:

$$\alpha_{\beta r} = \frac{1}{\psi_m(T_1)}\left[\frac{\psi_m(T_2) - \psi_m(T_1)}{T_2 - T_1}\right] \tag{25}$$

Fig. 1 depicts the flux linkage references at $25°C$, $50°C$, $75°C$, $100°C$, and $125°C$, respectively, along with $\alpha_{\beta r}$ calculated using two adjacent temperature points. These values are selected for the estimation at each temperature region. The difference in $\alpha_{\beta r}$ may be associated with the attribute of the material for the magnets.

The rotor temperature estimation errors at various motor speeds and temperatures shown in Fig. 12, are plotted in Fig. 13. Approximately 10℃ maximum deviation is the result of the error in the estimated flux linkage at low speed.

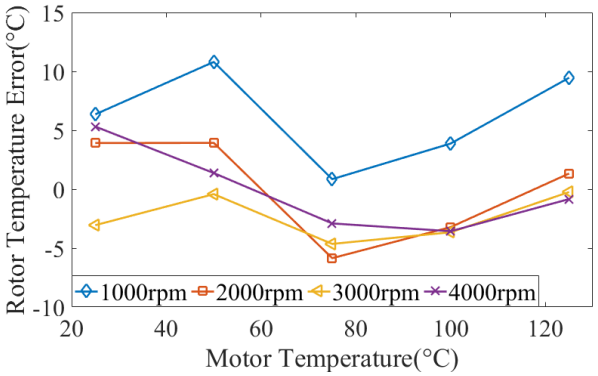

Fig. 13: Rotor temperature errors at 1000rpm, 2000rpm, 3000rpm, 4000rpm, and rising temperatures

A thermal transient test over four hours is performed in which the motor temperature increases and decreases in steps generated by temperature controller, as Fig. 14(a) illustrates. The setup shown in Fig. 10 is employed, such that at thermal steady state, the rotor temperature is assumed to be identical to the winding temperature and the difference between them considered the estimation error. In order to validate the presented method in non-stationary conditions, a simplified duty cycle is applied to speed and stator current and shown in Fig. 14(b).

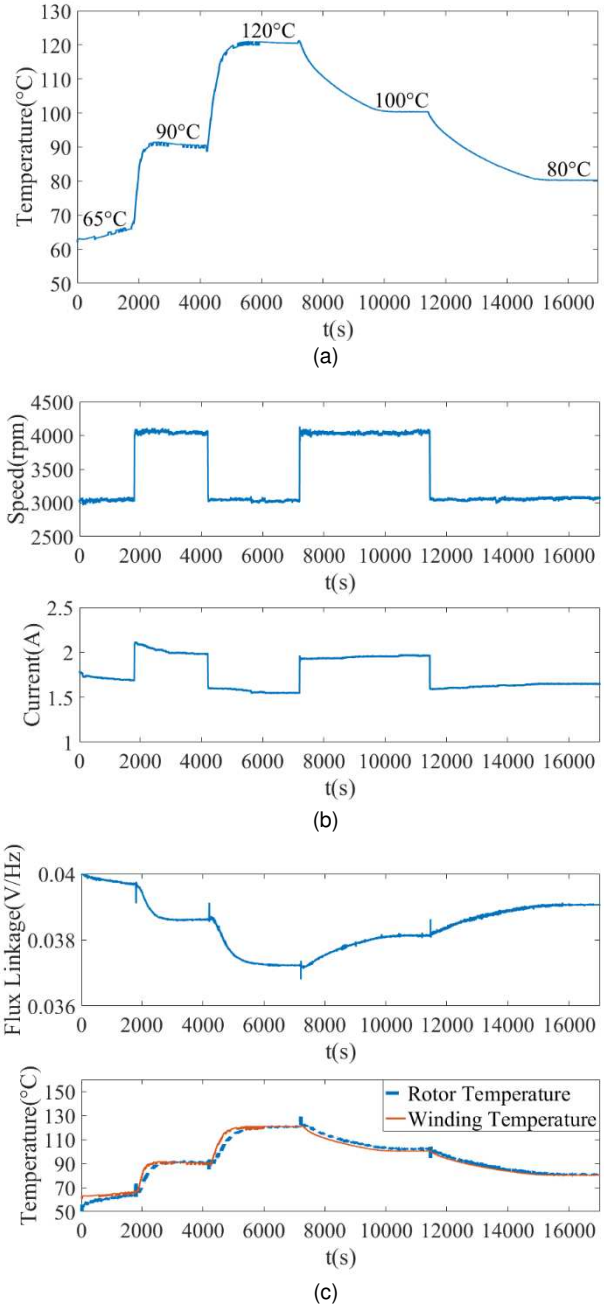

Fig. 14: (a) Motor temperature profile during transient testing (b) Motor speed and current profiles of the transient testing and (c) Flux linkage (top) and rotor temperature (bottom) estimations under the transient profiles

Less than $1.7°C$ differences in the converged step temperatures between winding and rotor can be observed in Fig. 14(c). The estimation error is rather modest, as the error in flux linkage is less than $0.3\% - 0.4\%$ at high motor temperature, according to Fig. 12. It is worth noticing that, the same flux linkage error at high motor temperature will lead to smaller error in the estimation of the rotor temperature, due to the value of the coefficient $\alpha_{\beta r}$ increasing with temperature, as Fig. 1 suggests.

However during transient, the winding temperature cannot be used as the reference to the estimation, because the thermal time constant of the motor stator winding is smaller than that of the rotor, based on the simulation results generated by the Finite Element software Motor-CAD and shown in Fig. 15. It can be explained by the fact that for the motor under test, a thermal resistance between the stator and rotor exists and also in this application, the external power from the heater mats flows from the stator through the air gap to the rotor. These effects lead to a faster stator temperature change. This is consistent with Fig. 14(c). In this application, it is impractical to install temperature sensors directly on the rotor for the measurement of the reference.

Also, the heater mat is slightly shorter in length than the motor circumference. Therefore, the heating distribution in the motor might not be uniform. Additionally, rotor temperature is indirectly measured using stator windings temperature and assuming adiabatic and steady-state conditions, assuming that in these conditions stator and rotor have reached a thermal equilibrium. These ideal conditions might not be perfectly verified in practice.

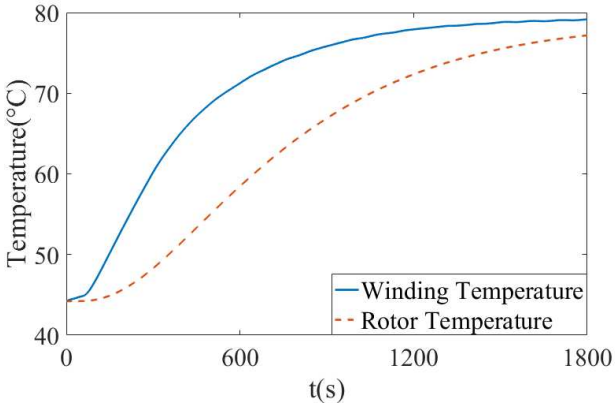

Fig. 15: Motor stator winding and rotor temperatures during transient period acquired from the FE software Motor-CAD

V. Conclusion

This paper presents a relatively simple and accurate method for online flux linkage and rotor temperature estimations of PMSMs, based on the current response to the standard SV-PWM which is commonly employed in most state-of-the-art power converter drive applications. This method is simple to implement and does not require additional hardware neither creates additional disturbance to the machine as no additional signal injection is required. The method is also independent of

machine inductances. Extensive simulations and experimental tests validating the proposed methodology on a typical SPMSM, are provided to evaluate the sensitivity and robustness of the method to a number of parameters including dead-time, saturation and non-zero *d*-current. The results demonstrate good accuracy in rotor flux linkage and temperature estimations in a wide range of machine operating conditions.

REFERENCES

[1] T. Huber, W. Peters, and J. Bocker. "A low-order thermal model for monitoring critical temperatures in permanent magnet synchronous motors," in *Proc. 7th IET Conf. Power Electron. Mach. Drives*, pp. 1-6, Oct. 2014.

[2] A. Specht and J. Bocker. "Observer for the rotor temperature of IPMSM," in *Proc. 14th Int. Power Electron. Motion Control Conf.*, pp. T4-12 – T4-15, Sep. 2010.

[3] J. Dymond, R. Ong, and N. Stranges, "Instrumentation, testing and analysis of electric machine rotor steady-state heating," *Petro. Chem. Ind. Conf., IEEE Ind. Appl. Soc. 48th Annu.*, pp. 297-303, Sept 2001.

[4] D. Reigosa, F. Briz, P. Garcia, J. M. Guerrero, and W. Degner, "Magnet temperature estimation in surface PM Machines using high-frequency signal injection," *IEEE Trans. Ind. Appl.*, vol. 46, no. 4, pp. 1468–1475, Jul./Aug. 2010.

[5] D. Reigosa, F. Briz, M. W. Degner, P. García, and J. M. Guerrero, "Magnet temperature estimation in surface PM machines during six-step operation," *IEEE Trans. Ind. Appl.,* vol. 48, no. 6, pp. 2353–2361, Nov./Dec. 2012.

[6] Z. Hou and G. Gu, "Wireless rotor temperature measurement system based on MSP430 and nRF401," in *Proc. Int. Conf. Electrical Mach. Systems, ICEMS 2008*, pp. 858-861, Oct. 2008.

[7] D. Fernandez, D. Reigosa, T. Tanimoto, T. Kato, and F. Briz, "Wireless permanent magnet temperature and field distribution measurement system for IPMSMs," in *Proc. IEEE Energy Convers. Cong. Expo.,* pp. 3996-4003, Sept. 2015.

[8] G. D. Demetriades, H. Z. de la Parra, E. Andersson, and H. Olsson, "A real-time thermal model of a permanent-magnet synchronous motor," *IEEE Trans. Power Electron.*, vol. 25, no. 2, pp. 463–474, Feb. 2010.

[9] X. Chen, J. Wang, and A. Griffo, "A high-fidelity and computationally efficient electro-thermally coupled model for interior permanent-magnet machines in electric vehicle traction applications*," IEEE Trans. Transport. Electrific.,* vol. 1, no. 4, pp. 336–347, Dec. 2015.

[10] C. Kral, A. Haumer, and S. B. Lee, "A practical thermal model for the estimation of permanent magnet and stator winding temperatures," *IEEE Trans. Power Electron.*, vol. 29, no. 1, pp. 455-464, Jan. 2014.

[11] O. Wallscheid and J. Bocker. "Design and empirical identification of a lumped parameter thermal network for permanent magnet synchronous motors with physically motivated constraints", in *Proc. IEEE Int. Electric Mach. Drives Conf.*, Feb. 2016.

[12] O. Wallscheid and J. Bocker. "Global identification of a low-order lumped-parameter thermal network for permanent magnet synchronous motors", *IEEE Trans. Energy Convers.*, vol. 31, no. 1, pp. 354–365, Sept. 2016.

[13] D. Reigosa, D. Fernandez, H. Yoshida, T. Kato, and F. Briz, "Permanent-magnet temperature estimation in PMSMs using pulsating high-frequency current injection*," IEEE Trans. Ind. Appl.*, vol. 51, no. 4, pp. 3159–3168, Jul-Aug. 2015.

[14] M.-D. Calin and E. Helerea, "Temperature influence on magnetic characteristics of NdFeB permanent magnets," in *Proc. 7th Int. Symp. Adv. Topics Electrical Eng,*, pp. 1-6, May 2011.

[15] K. Liu, Z. Zhu, and D. Stone. "Parameter estimation for condition monitoring of PMSM stator winding and rotor permanent magnets", *IEEE Trans. Ind. Electron.*, vol. 60, no. 12, pp. 5902–5913, Dec. 2013.

[16] K. W. Lee, D. H. Jung, and I. J. Ha, "An online identification method for both stator resistance and back-EMF coefficient of PMSMs without rotational transducers," *IEEE Trans. Ind. Electron.*, vol. 51, no. 2, pp. 507-510, Apr. 2004.

[17] S. Morimoto, M. Sanada, and Y. Takeda, "Mechanical sensorless drives of IPMSM with online parameter identification," *IEEE Trans. Ind. Appl.*, vol. 42, no. 5, pp. 1241-1248, Sep.-Oct. 2006.

[18] S. J. Underwood and I. Husain, "Online parameter estimation and adaptive control of permanent magnet synchronous machines," *IEEE Trans. Ind. Electron.*, vol. 57, no. 7, pp. 2435-2443, Jul. 2010.

[19] G. Xie, K. Lu, S. K. Dwivedi, R. J. Riber, and W. Wu. "Permanent magnet flux online estimation based on zero-voltage vector injection method", *IEEE Trans. Power Electron.*, vol. 30, no. 12, pp. 6506–6509, Dec. 2015.

[20] A. Specht, O. Wallscheid, and J. Bocker, "Determination of rotor temperature for an interior permanent magnet synchronous machine using a precise flux observer," in *Proc. Int. Power Electron. Conf.*, pp. 1501-1507, May 2014.

[21] O. Wallscheid, A. Specht, and J. Bocker. "Observing the permanent magnet temperature of synchronous motors based on electrical fundamental wave model quantities", *IEEE Trans. Ind. Electron.*, vol. 64, no. 5, pp. 3921–3929, May 2017.

[22] T. Senjyu, Y. Kuwae, N. Urasaki, and K. Uezato, "Accurate parameter measurement for high speed permanent magnet," in *Proc. 2nd Int. Conf. Power Electron. Mach. Drives*, pp. 772-777, Jun. 2001.

[23] R. Ramakrishnan, R. Islam, M. Islam, and T. Sebastian, "Real time estimation of parameters for controlling and monitoring permanent magnet synchronous motors," in *Proc. IEEE Int. Electric Mach. Drives Conf.*, pp. 1194-1199, May 2009.

[24] Z. Zhu, X. Zhu, P. Sun, and D. Howe, "Estimation of winding resistance and PM flux-linkage in brushless AC machines by reduced-order extended Kalman Filter," in *Proc. IEEE Int. Conf. Netw. Sens. Control*, pp. 740-745, Apr. 2007.

[25] S. Xiao and A. Griffo. "PWM-based flux linkage estimation for permanent magnet synchronous machines," in *Proc. 9th IET Conf. Power Electron. Mach. Drives,* pp. 1-6, Apr. 2018.

[26] B. K. Bose, *Modern power electronics and AC drives*, 1st ed., ser. 1. Upper Saddle River: Prentice Hall PTR, ch. 5, pp. 224-229, 2002.

[27] N. Takahashi, M. Morishita, D. Miyagi and M. Nakano, "Examination of magnetic properties of magnetic materials at high temperature using a ring specimen," *IEEE Trans. Magn.*, vol. 46, no. 2, pp. 548-551, Feb. 2010.

[28] M. Morishita, N. Takahashi, D. Miyagi and M. Nakano, "Examination of magnetic properties of several magnetic materials at high temperature," *Przeglad Elektrotechniczny (Electrical Review)*, vol. 87, no. 9b/2011, pp. 106-110, 2011.

Shuai Xiao received the M.Sc. degree in electrical power from Newcastle University, Newcastle, U.K., and the Ph.D. degree in electrical and electronic engineering from the University of Sheffield, Sheffield, U.K., in 2014 and 2019, respectively.

His current research interests include thermal modelling, hardware-in-the-loop emulation, and online temperature monitoring of permanent magnet synchronous machines for traction applications.

Antonio Griffo (M'13) received the M.Sc. degree in electronic engineering and the Ph.D. degree in electrical engineering from the University of Napoli "Federico II," Naples, Italy, in 2003 and 2007, respectively.

From 2007 to 2013, he worked as a research associate at the University of Sheffield, Sheffield, U.K., and the University of Bristol, Bristol, U.K. He is currently a senior lecturer in the Department of Electronic and Electrical Engineering, the University of Sheffield. His research interests include modelling, control, and condition monitoring of electric power systems, power electronics converters, and electrical motor drives for renewable energy, automotive, and aerospace applications.